Visualizing molecular weights differences in supramolecular polymers

Qingyun Li[a], Hanwei Zhang[a], Kai Lou[a], Yabi Yang[a], Xiaofan Ji[a,1], Jintao Zhu[a,1], and Jonathan L. Sessler[b,1]

[a]Key Laboratory of Materials Chemistry for Energy Conversion and Storage, Ministry of Education, Hubei Key Laboratory of Materials Chemistry and Service Failure, School of Chemistry and Chemical Engineering, Huazhong University of Science and Technology, Wuhan 430074, China; and [b]Department of Chemistry, The University of Texas at Austin, Austin, TX 78712

Contributed by Jonathan L. Sessler; received November 30, 2021; accepted January 12, 2022; reviewed by Hai-Bo Yang and Yanli Zhao

Issues of molecular weight determination have been central to the development of supramolecular polymer chemistry. Whereas relationships between concentration and optical features are established for well-behaved absorptive and emissive species, for most supramolecular polymeric systems no simple correlation exists between optical performance and number-average molecular weight (M_n). As such, the M_n of supramolecular polymers have to be inferred from various measurements. Herein, we report an anion-responsive supramolecular polymer $[M1{\cdot}Zn(OTf)_2]_n$ that exhibits monotonic changes in the fluorescence color as a function of M_n. Based on theoretical estimates, the calculated average degree of polymerization (DP_{cal}) increases from 16.9 to 84.5 as the monomer concentration increases from 0.08 mM to 2.00 mM. Meanwhile, the fluorescent colors of M1 + $Zn(OTf)_2$ solutions were found to pass from green to yellow and to orange, corresponding to a red shift in the maximum emission band (λ_{max}). Therefore, a relationship between DP_{cal} and λ_{max} could be established. Additionally, the anion-responsive nature of the present system meant that the extent of supramolecular polymerization could be regulated by introducing anions, with the resulting change in M_n being readily monitored via changes in the fluorescent emission features.

supramolecular polymers | molecular weight | fluorescence | *J*-aggregate | self-assembly

Issues of molecular weight determination have been central to the development of polymer chemistry and date back, in fact, to the earliest days of the field and the controversies Staudinger faced (1, 2). The number-average molecular weight (M_n) of polymeric materials has a direct effect on their mechanical properties (1–3). Typically, the higher the molecular weight of the polymer, the greater its hardness and strength, as exemplified by polyethylene (4, 5). Therefore, determining the molecular weight of a polymeric material is often a first key step in its characterization. Being able to do so simply could be particularly advantageous in the case of supramolecular polymers where the degree of polymerization, and hence molecular weight, can vary as a function of conditions. Supramolecular polymers, unlike conventional polymers, are polymeric arrays of repeat units that are held together by directional noncovalent interactions (6, 7). Given the reversible noncovalent bonds embodied in supramolecular polymers, they typically exhibit not only polymer-like properties as bulk materials and in solution, but also dynamic characteristics. These latter attributes often have no parallel in the case of covalent polymers and include *inter alia* reversible formation, recyclability, and stimulus responsiveness (8–26), including to anions whose role in the fields of biology, chemistry, energy, and supramolecular chemistry is well appreciated (27–42). These key features complicate molecular weight determinations, as does the fact that a distribution of molecular weights around an average is generally observed. Moreover, due to the dynamic nature of noncovalent bonds, the monomers used to create supramolecular polymers can assemble in a variety of aggregation modes (7, 39). For instance, when the monomer concentration is low, cyclic species or oligomers are more likely to form. However, at concentrations greater than the so-called critical polymer concentration (CPC), appropriately designed monomers will assemble to form supramolecular polymers, whose M_n typically grows with monomer concentration. As a consequence, the M_n of supramolecular polymers generally reflects the constituent monomer concentration(s).

Whereas relationships between concentration and optical features are established for well-behaved absorptive and emissive species (e.g., monomeric compounds that obey the Beer–Lambert or Beer–Lambert–Bouguer laws), for most polymeric systems no simple correlation exists between easy-to-monitor optical properties, such as fluorescence emission color, and the molecular weight. As such, the molecular weights of supramolecular polymers have to be inferred from less-direct measurements (43–45). For example, the average degree of supramolecular polymerization can be calculated (DP_{cal}) by measuring the equilibrium constant of the interaction between monomers and applying various theoretical models (39, 46, 47). Alternatively, in certain cases the molecular weights of supramolecular polymers can be deduced empirically from the intrinsic viscosities using the Mark–Houwink equation (48, 49). Vapor pressure osmometry measurements, which rely on the relationship between molecular weight and vapor pressure

Significance

Molecular weight determinations play a vital role in the characterization of supramolecular polymers. They are essential to assessing the degree of polymerization, which in turn can have a significant impact on the properties of the polymer. While numerous characterization methods have been developed to estimate the number-average molecular weight (M_n) of supramolecular polymers, a simple visual method could provide advantages in terms of ease of use. We have now developed a system wherein differences in the fluorescent signature, including changes in color, allow variations in the M_n of an anion-responsive supramolecular polymer $[M1{\cdot}Zn(OTf)_2]_n$ to be readily monitored. The present visual differentiation strategy provides a tool that may be used to characterize supramolecular polymers.

Author contributions: Q.L., X.J., and J.L.S. designed research; Q.L. performed research; X.J., J.Z., and J.L.S. analyzed data; and Q.L., H.Z., K.L., Y.Y., X.J., J.Z., and J.L.S. wrote the paper.

Reviewers: H.-B.Y., East China Normal University; and Y.Z., Nanyang Technological University.

The authors declare no competing interest.

[1]To whom correspondence may be addressed. Email: xiaofanji@hust.edu.cn, jtzhu@mail.hust.edu.cn, or sessler@cm.utexas.edu.

This article contains supporting information online at http://www.pnas.org/lookup/suppl/doi:10.1073/pnas.2121746119/-/DCSupplemental.

Published February 23, 2022.

(Raoult's law), can be used to deduce the molar mass of supramolecular polymers (50, 51). Matrix-assisted laser desorption ionization time-of-flight mass spectrometry has also been exploited to characterize oligomers and various relatively small self-assembled ensembles (52, 53). The molecular weights (M_n) of supramolecular polymers can also be inferred from concentration-dependent chemical shift changes in the corresponding ^{1}H NMR spectra (54). Separately, single-molecule force spectroscopy experiments have been used to determine the length of the bridges between the tip and substrate formed by supramolecular polymers, thus providing insights into the effective molecular weight of the polymer (55). These techniques notwithstanding, there remains a need for simple methods that would allow changes in the molecular weight of supramolecular polymers to be determined by optical means. Here, we report a system where a simple correlation is established between the fluorescence emission features and the M_n of a supramolecular polymer.

The present approach is based on an appreciation that *J*-type dyes have been identified in a variety of aggregation modes (56–59), including monomer, dimer, and stacked arrangements. Dyes of this type, which include a number of polycyclic and heterocyclic aromatic molecules, typically display fluorescent colors that vary as a function of concentration. Therefore, we postulated that incorporating *J*-type dyes into appropriately chosen monomers would endow the resulting putative supramolecular polymers with variable fluorescent colors, the specifics of which could be correlated with the degree of polymerization (Fig. 1). With such thinking in mind, we synthesized monomer **M1** by modifying a *J*-type dye, naphthalene diimide (NDI) (60, 61), with two alkylated terpyridine derivatives at both ends (Fig. 1). The NDI-derived **M1** interacts with $Zn(OTf)_2$ in DMF/H_2O (1/4, vol/vol) solution through terpyridine–Zn^{2+} coordination. At low monomer concentrations, these two components were expected to self-assemble into cyclic species or short oligomers characterized by long distances between the NDI subunits. Thus, little stacking would be seen, resulting in a green, monomer-dominated fluorescence for dilute **M1** + $Zn(OTf)_2$ solutions. As the total monomer concentration is increased with the ratio of **M1** and $Zn(OTf)_2$ kept constant at 1:1, the cyclic species would be expected to transform gradually into linear supramolecular polymers, [**M1**·$Zn(OTf)_2$]$_n$. Under these conditions, a limited degree of interchain association (e.g., the formation of double-strand dimers) is expected, leading to a decrease in the distance between NDI groups and a change in the fluorescent color from green to yellow. Upon increasing the monomer concentration, a corresponding increase in the polymer chain length is expected, which will lead to tight entanglement between individual polymer chains, further reducing the average distance between the emissive NDI groups. In the limit, this reduction in inter-NDI spacing would lead to formation of *J*-aggregates, which in the case of the NDI-containing **M1** component would give rise to orange-colored fluorescence. In accord with prior work involving supramolecular systems (27, 38), we also appreciated that anion recognition could be used to adjust the molecular weight of the supramolecular polymers formed from **M1** and $Zn(OTf)_2$. Specifically, we expected that adding tetraethylammonium hydroxide (TBAOH) to [**M1**·$Zn(OTf)_2$]$_n$ would lead to depolymerization as the result of complexation between the OH^- anions and Zn^{2+}. This would lead to restoration of the initial emission color. As detailed below, these design expectations were realized. Specifically, the M_n of the supramolecular aggregates formed from **M1** and $Zn(OTf)_2$ produced in dimethylformamide (DMF)/H_2O (1/4, vol/vol) solution could be distinguished by monitoring the fluorescent colors as a function of **M1** + $Zn(OTf)_2$ and TBAOH concentration.

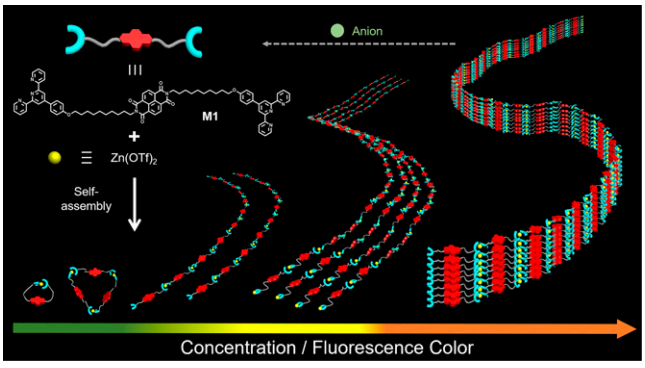

Fig. 1. Schematic representation of the anion-responsive supramolecular polymer of this study. Chemical structure of supramolecular monomers and cartoon representations of the proposed supramolecular polymerization process and anion-responsive behavior and the various fluorescent colors expected as the degree of intermonomer interaction increases.

Results and Discussion

Synthesis of M1 and Preparation of M1 + Zn(OTf)$_2$ Solutions. The synthetic procedure used to access monomer **M1** is shown in *SI Appendix*, Fig. S1. **M1** and its precursors were characterized by means of ^{1}H NMR spectroscopy, ^{13}C NMR spectroscopy, and high-resolution mass spectrometry (*SI Appendix*, Figs. S2–S13). To prepare **M1** + $Zn(OTf)_2$ solutions (*SI Appendix*, Fig. S14), equimolar solutions of monomer **M1** and $Zn(OTf)_2$ were made up in chloroform (1.25 mL) and methanol (1.25 mL), respectively. These two solutions were then combined and stirred for 1 h at 298 K. The resulting mixture was subject to slow evaporation at 298 K giving **M1**·$Zn(OTf)_2$ as a solid, which subsequently was dissolved in DMF/H_2O (1/4, vol/vol) to give a stock solution of **M1** + $Zn(OTf)_2$ (2.00 mM, 500 μL). Standard solutions of **M1** + $Zn(OTf)_2$ (0.08 to 1.80 mM) were then prepared by diluting this **M1** + $Zn(OTf)_2$ stock solution (2.00 mM) with DMF/H_2O (1/4, vol/vol). Note that the concentrations of **M1** + $Zn(OTf)_2$ mentioned in this article refer to the total monomer concentration [i.e., the sum of the **M1** + $Zn(OTf)_2$ concentrations]. Unless otherwise noted, the ratio of **M1** and $Zn(OTf)_2$ was held constant at 1:1.

Job Plots and Ultraviolet-Visible Spectroscopic Titrations. To obtain insights into the interactions between **M1** and $Zn(OTf)_2$, the complexation between precursor **1a** (Fig. 2*A*) and $Zn(OTf)_2$ was studied using the Job method (62–64). As shown in Fig. 2*A*, an adsorption peak for **1a** in DMF/H_2O (1/4, vol/vol) was observed at 285 nm, whose intensity decreased as the molar ratio of [$Zn(OTf)_2$]/([$Zn(OTf)_2$] + [**1a**]) increased. An absorbance feature at 340 nm was also seen that increased in intensity initially but then declined as the molar ratio of [$Zn(OTf)_2$]/([$Zn(OTf)_2$] + [**1a**]) increased. The changes in the absorbance at 340 nm were plotted against the molar ratio of [$Zn(OTf)_2$]/([$Zn(OTf)_2$] + [**1a**]) to give a Job's plot (Fig. 2*B*) (63). This plot revealed an absorbance maximum when the mole fraction of [$Zn(OTf)_2$] was 0.33. While not a proof, this finding is consistent with a 1:2 binding stoichiometry in this solvent system, wherein each Zn^{2+} ion complexes two molecules of **1a**.

The binding between compound **1a** and $Zn(OTf)_2$ was further studied by means ultraviolet-visible (UV-vis) spectroscopic titrations (Fig. 2*C*) (65). Upon the addition of $Zn(OTf)_2$ to a dilute solution of **1a** in DMF/H_2O (1/4, vol/vol), a decline in the original adsorption peak at 285 nm is seen. Concurrently, a new peak at 340 nm is seen to grow in. This latter spectral feature is attributed to the formation of octahedral complexes characterized by distinct metal–ligand charge transfer bands (66). Titration curves were constructed by plotting

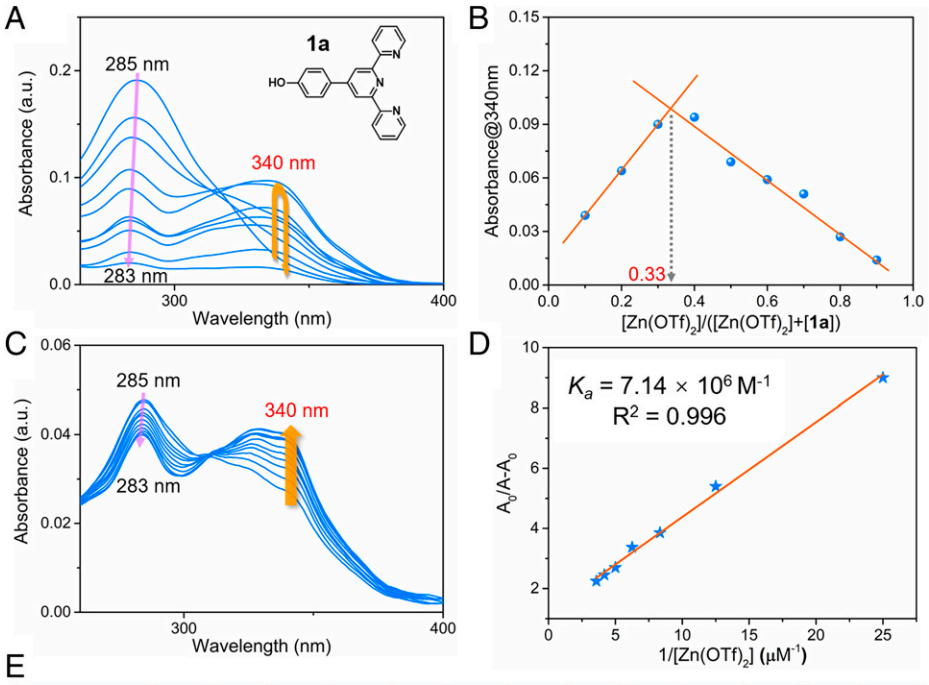

E

[Monomer] (mM)	0.08	0.12	0.16	0.20	0.40	0.60	0.80	1.00	1.20	1.40	1.60	1.80	2.00
DP_{cal}	16.9	20.7	23.9	26.7	37.8	46.3	53.4	59.7	65.4	70.7	75.6	80.2	84.5

Fig. 2. Complexation study and degree of polymerization calculation. (*A*) UV-vis spectra of mixtures of $Zn(OTf)_2$ and **1a** in DMF/H_2O (1/4, vol/vol) at different molar ratios. The total concentration of **1a** and $Zn(OTf)_2$ was kept at 5.00 μM. (*Inset*) chemical structure of compound **1a**. (*B*) Job's plot of compound **1a** and $Zn(OTf)_2$. (*C*) UV-vis spectra of compound **1a** (0.280 μM) in 1.00 mL DMF/H_2O (1/4, vol/vol) recorded upon the stepwise addition of $Zn(OTf)_2$ (100 μM) at 298 K. (*D*) Plot of $(A_0/(A - A_0)$ as a function of 1/[$Zn(OTf)_2$]. The apparent association constant K_a corresponding to the interaction between **1a** (0.280 μM) and $Zn(OTf)_2$ (100 μM) was determined using the Benesi–Hilderbrand equation $A_0/(A - A_0) = (A_0/(A_{max} - A_0))((1/K_a)\ [Zn(OTf)_2]^{-1} + 1)$. (*E*) The degree of polymerization calculated (DP_{cal}) for equimolar mixtures of **M1** and $Zn(OTf)_2$ (0.08 to 2.00 mM).

the absorbance values at 340 nm versus the $Zn(OTf)_2$ concentration (*SI Appendix*, Fig. S15). A positive correlation between the absorbance intensity at 340 nm and the $Zn(OTf)_2$ concentration was seen over the 0.00 to 1.00 equiv. concentration range. However, adding further quantities of $Zn(OTf)_2$ produced no appreciable changes in the absorbance intensity at 340 nm. The relationship between the absorbance at 340 nm and the $Zn(OTf)_2$ concentration (0.00 to 1.00 equiv.) could be linearized according to the Benesi–Hildebrand equation (67, 68), allowing a binding constant, K_a, of $7.14 \times 10^6\ M^{-1}$, corresponding to the interaction **1a** and $Zn(OTf)_2$, to be estimated (Fig. 2*D*). Compound **1a** containing one terpyridine can complex with $Zn(OTf)_2$ in a 2:1 manner. In contrast to compound **1a**, monomer **M1**, which includes two terpyridines, can self-assemble with $Zn(OTf)_2$ in a net 1:1 stoichiometry to form supramolecular polymers at high concentrations. Thus, the binding constant of **1a** and $Zn(OTf)_2$ can be used to calculate the DP_{cal} of the supramolecular polymer, $[\mathbf{M1}{\cdot}Zn(OTf)_2]_n$. This value was then substituted into the equation $DP \approx (K_aC)^{1/2}$ to obtain a relationship between the DP_{cal} and the monomer concentration (Fig. 2*E*) (54, 69). Based on the model studies with **1a**, it was expected that increasing the total concentration of an equimolar mixture of **M1** and $Zn(OTf)_2$ from 0.08 mM to 0.20 mM would lead to a corresponding increase in the DP_{cal} from 16.9 to 26.7 (Fig. 2*E*). Likewise, as the concentration of **M1** + $Zn(OTf)_2$ increased from 0.40 mM to 2.00 mM, the calculated DP_{cal} rises from 37.8 to 84.5 (Fig. 2*E*). The theoretical model was also successfully applied to the characterization of molecular weights for similar metallo-supramolecular polymers based on other metal ions, including Fe(II), Cu(II), Co(II), Cd(II), and Ni(II) (*SI Appendix*, Figs. S16–S20).

Viscosity Method. To provide evidence that a supramolecular polymer, $[\mathbf{M1}{\cdot}Zn(OTf)_2]_n$, was formed from a mixture of **M1** and $Zn(OTf)_2$, we determined the specific viscosity of various **M1** + $Zn(OTf)_2$ solutions (0.08 to 2.00 mM) (70, 71). A double logarithmic plot of the specific viscosity versus the **M1** + $Zn(OTf)_2$ concentration was then constructed (*SI Appendix*, Fig. S21). As the total concentration of these two monomers increased from 0.08 to 0.20 mM, the specific viscosity rose steadily with a slope of 0.256. When the total concentration of **M1** + $Zn(OTf)_2$ was increased past 0.40 mM, there was a dramatic increase in the specific viscosity, with a slope of 1.14 being seen. The concentration of **M1** + $Zn(OTf)_2$ corresponding to the intersection of two fitted linear lines (0.22 mM) was defined as the CPC (70). The slope in the low concentration range reflects the characteristics of cyclic species or oligomers expected in dilute solutions. Conversely, the dramatic increase in the specific viscosity seen above the CPC is ascribed to the formation of linear supramolecular polymers and the entanglement between individual linear polymers. Therefore, these results support the design expectation that supramolecular polymers would form at high total monomer concentrations, while relatively small oligomers would form at lower monomer concentrations.

Scanning Electron Microscopic, Atomic Force Microscopic, and Laser Scanning Confocal Microscopic Studies of Equimolar Mixtures of M1 and $Zn(OTf)_2$. Additional evidence for the formation of supramolecular polymers of generalized structure $[\mathbf{M1}{\cdot}Zn(OTf)_2]_n$ came from morphology experiments (72). Scanning electron microscopic (SEM) images of **M1** + $Zn(OTf)_2$ determined at different concentrations of **M1** + $Zn(OTf)_2$ are shown in Fig. 3*A*. At total concentrations below 0.20 mM, only particle-like structures are

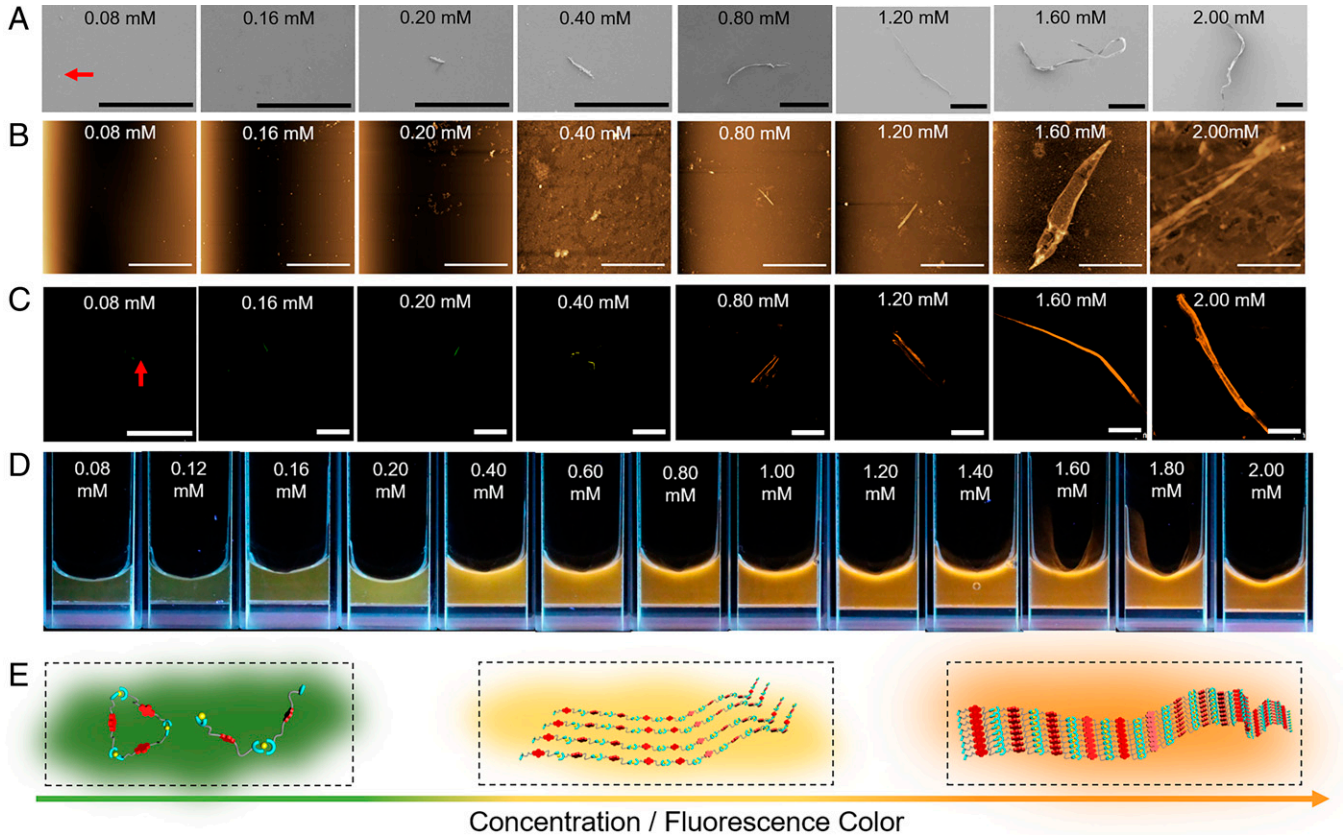

Fig. 3. Morphology, fluorescence behavior, and proposed determinants of the observed **M1** + $Zn(OTf)_2$ emission colors. (*A*) SEM images, (*B*) AFM images, and (*C*) LSCM images of the equimolar mixtures of **M1** and $Zn(OTf)_2$ at different concentrations (0.08, 0.16, 0.20, 0.40, 0.80, 1.20, 1.60, and 2.00 mM in DMF/H_2O (1/4, vol/vol)). λ_{ex} = 405 nm. (*D*) Photographs of equimolar mixtures of **M1** and $Zn(OTf)_2$ (0.08 to 2.00 mM) under UV light. (*E*) Cartoon representations of the self-assembly process thought to govern equimolar mixtures of **M1** and $Zn(OTf)_2$ and the change in the fluorescence color observed as the concentration is increased. (Scale bars: *A*, 200 μm; *B*, 20.0 μm; *C*, 100 μm.)

observed. However, fibrous structures (73) are seen when the total concentration reached 0.20 mM. The length of these fibers was seen to grow as the monomer concentration was increased further from 0.20 mM to 2.00 mM, as would be expected given the proposed formation of $[\mathbf{M1}{\cdot}Zn(OTf)_2]_n$.

Atomic force microscopy (AFM) is another powerful tool that may be used to determine the morphology of self-assembled materials (74). Thus, $[\mathbf{M1}{\cdot}Zn(OTf)_2]_n$ was analyzed at different monomer concentrations via tapping-mode AFM (75). Consistent with the images captured through SEM, microsized particles were observed by AFM over the 0.08 mM to 0.16 mM monomer concentration regime, while fibrous species of increasing size were seen as the monomer concentration was increased past 0.20 mM; this was accompanied by a decrease in the number of visible particles (Fig. 3*B*). Again, these findings were taken as evidence that short oligomers are produced at relatively low monomer concentrations, while supramolecular polymers are formed at high monomer concentrations (74, 76).

Laser scanning confocal microscopy (LSCM) was used to probe the change in fluorescence and morphological characteristics as the total concentration of **M1** + $Zn(OTf)_2$ in DMF/H_2O (1/4, vol/vol) was varied (77, 78). The resulting outputs of LSCM were obtained as digital false-color images (77). The fluorescence colors shown for the LSCM images (Fig. 3*C*) were then generated using the fluorescence colors of **M1** + $Zn(OTf)_2$ solutions under UV excitation (hand-held lamp; 365 nm) (Fig. 3*D*). As shown in Fig. 3*C*, microsized particles were observed at a total monomer concentration of 0.08 mM. As the monomer concentration increased, fibrous species first appeared and then increased in size. A concurrent change in the color of the samples was also observed, revealing distinct differences in the fluorescence properties as a function of the dynamic assembly process. Notably, as the monomer concentration was raised from 0.08 mM to 0.16 mM, the fluorescent color of the samples evolved, changing from dark green to green. When the total monomer concentration reached 0.40 mM (corresponding to formation of a fibrous structure) a yellow fluorescence was seen. An orange fluorescence was seen at **M1** + $Zn(OTf)_2$ concentrations over 0.40 mM. These findings thus provided an initial indication that a useful relationship might exist between the monomer concentration and the fluorescence features of the self-assembled species formed from 1:1 mixtures of **M1** and $Zn(OTf)_2$.

Fluorescence Properties of Equimolar Mixtures of M1 and $Zn(OTf)_2$. To test the presumed relationship between monomer concentration and the fluorescence emission in our system, we monitored the colors of 1:1 **M1** + $Zn(OTf)_2$ solutions in DMF/H_2O (1/4, vol/vol) at different total monomer concentrations under UV excitation. As shown in Fig. 3*D* and Movie S1, as the monomer concentration increased different colors were observed. In accord with the LSCM study above, the colors evolved from green to yellow and then to orange with increasing **M1** + $Zn(OTf)_2$ concentration.

Fig. 3*E* shows in cartoon fashion our proposed mechanistic rationale for the observed fluorescent color changes. At low total monomer concentrations (0.08 to 0.20 mM), **M1** and $Zn(OTf)_2$ self-assemble to form cyclic species or oligomers. Under these conditions, the probability of contact between **M1** subunits is low, resulting in a large separation between the emissive NDI groups. Thus, a monomer-like green NDI-based

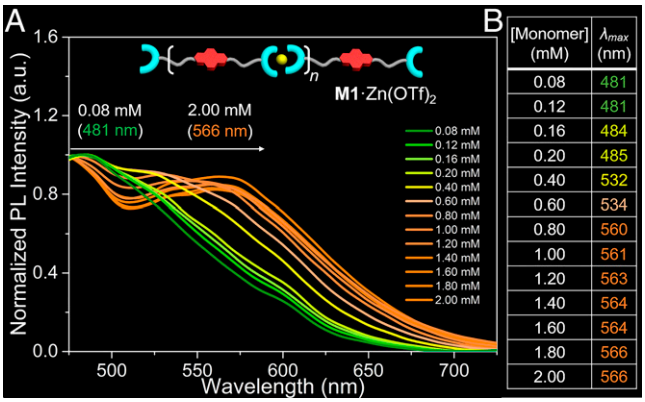

[Monomer] (mM)	λ_{max} (nm)
0.08	481
0.12	481
0.16	484
0.20	485
0.40	532
0.60	534
0.80	560
1.00	561
1.20	563
1.40	564
1.60	564
1.80	566
2.00	566

Fig. 4. Fluorescence characterization of [**M1**·Zn(OTf)$_2$]$_n$ (*A*) Normalized fluorescent spectra of equimolar mixtures of **M1** and Zn(OTf)$_2$ in the concentration range (0.08 to 2.00 mM in DMF/H$_2$O [1/4, vol/vol]) at 298 K. λ_{ex} = 410 nm. Slit: 10/15. (*B*) Table showing the relationship between λ_{max} and monomer concentration.

emission is seen. As the total monomer concentration approaches the CPC (0.22 mM), supramolecular polymers start to form, contributing to more chain-to-chain contacts. These contacts serve to reduce the distance between the NDI groups, prompting a change in the fluorescent color from green to yellow. A further increase in the monomer concentration (0.60 to 2.00 mM) leads to an increase in the polymer size and molecular weight and interchain entanglement; this further shortens the distance between the NDI groups and supports formation of *J*-aggregates characterized by an orange emission.

To quantify the relationship between color and monomer concentration the emission spectra of 1:1 solutions of **M1** and Zn(OTf)$_2$ were recorded as a function of total monomer concentration. Note that an excitation wavelength of 410 nm was used since cleaner spectra were obtained than when a 365 nm excitation (as used for the photographic studies above) was employed, The normalized emission spectra (475 to 725 nm) for these **M1** + Zn(OTf)$_2$ solutions over the 0.08 mM to 2.00 mM concentration range are shown in Fig. 4*A*. The corresponding emission maxima (λ_{max}) are shown in Fig. 4*B*. When the monomer concentration is increased from 0.08 mM to 0.20 mM, a shift of only 4 nm in λ_{max} from 481 nm to 485 nm is seen. This finding is consistent with the monomeric form of NDI dominating within this concentration regime. However, as the concentration reached 0.40 mM, a remarkable redshift in the λ_{max} to 532 nm was observed, a finding interpreted in terms of the formation of substantial quantity of the dimeric NDI form. At high concentrations (i.e., >0.60 mM), the λ_{max} shifts steadily from 534 nm to 560 nm as a function of concentration. This finding is interpreted in terms of larger-sized π-stacked structures dominating in this concentration regime. These results led us to infer that a dependent relationship between the monomer concentration and the observed λ_{max} pertains for solutions of **M1** + Zn(OTf)$_2$ (58, 79). Additionally, the emission spectra of these **M1** + Zn(OTf)$_2$ solutions were recorded over the 0.08 mM to 2.00 mM range and used to generate a Commission Internationale de l'Eclairage (CIE) diagram (*SI Appendix*, Fig. S23). This CIE diagram proved concordant with the colors shown in Fig. 3*D* (80).

Relationship between DP$_{cal}$ and the Maximum Emission Wavelength. The inferred dependent relationship between 1) the total monomer concentration and the DP$_{cal}$ (Fig. 2*E*) and 2) between the monomer concentration and the observed λ_{max} (Fig. 4*B*) allowed us to correlate the λ_{max} with DP$_{cal}$ as shown in Fig. 5. As the DP$_{cal}$ increases from 16.9 to 26.7 only a slight shift in λ_{max} from 481 nm to 485 nm is seen. In contrast, a dramatic shift in λ_{max} to 532 nm, corresponding to a DP$_{cal}$ of 37.8, was observed (Fig. 5*A*). A further remarkable shift in λ_{max} from 534 nm to 560 nm occurred as the DP$_{cal}$ rose from 46.3 to 53.4. As the DP$_{cal}$ was then increased to 84.5, a steady increase in the λ_{max} (from 560 nm to 566 nm) was seen (Fig. 5*A*). Additionally, the DP$_{cal}$ of the supramolecular polymer [**M1**·Zn(OTf)$_2$]$_n$ could be visually distinguished due to changes in the color of the solutions (Fig. 5*B*). Over the DP$_{cal}$ range of 16.9 to 26.7, the fluorescent color of the solutions changed slightly from dark green to green. Then, as the DP$_{cal}$ climbed to 37.8, a yellow fluorescence emission was observed, which changed to orange at a DP$_{cal}$ of 46.3, a color that deepened as the DP$_{cal}$ further increased to 84.5.

Preparation of Monomer M1 Solutions. Given that interactions between **M1** monomers that are independent of supramolecular polymer formation may contribute to the observed fluorescence behavior, the above tests were repeated for pure **M1** solutions under otherwise identical conditions. As above, an **M1** stock solution (1.00 mM) was prepared by dissolving **M1** in DMF/H$_2$O (1/4, vol/vol). Standard solutions of **M1** (0.04 to 0.90 mM) were then obtained by diluting this stock solution.

Viscosity Studies. The aggregation of **M1** was studied initially via viscosity tests. A double logarithmic plot of specific viscosity versus **M1** concentration is shown in *SI Appendix*, Fig. S22. In contrast to what was seen in the case of the corresponding **M1** + Zn(OTf)$_2$ solutions no pronounced changes in the slope were observed as a function of concentration; rather, the specific viscosities increased slowly over the full **M1** concentration range, with a slope of 0.151. Of note is that the slope (0.151) in the **M1** diagram is relatively close to the slope (0.256) recorded for **M1** + Zn(OTf)$_2$ solutions at relatively low concentration (0.04 to 0.20 mM). On this basis, we infer that only small-sized assemblies or nonsupramolecular polymer aggregates are formed from **M1** in DMF/H$_2$O (1/4, vol/vol) (64).

SEM, AFM, and LSCM Studies of M1. To explore further the aggregation modes of **M1** in DMF/H$_2$O (1/4, vol/vol), solutions of **M1** were subject to SEM, AFM, and LSCM analysis. In the SEM images (Fig. 6*A*), tiny particles were seen over the 0.04 mM to 0.10 mM **M1** concentration range. The size of these particles was seen to grow gradually as the concentration increased to 1.00 mM; however, no fibrous species were observed. This leads us to suggest that **M1** alone does not support the formation of supramolecular polymers. Consistent with this inference, only microsized particles were captured via AFM (Fig. 6*B*). The resulting LSCM outputs were treated as above to give

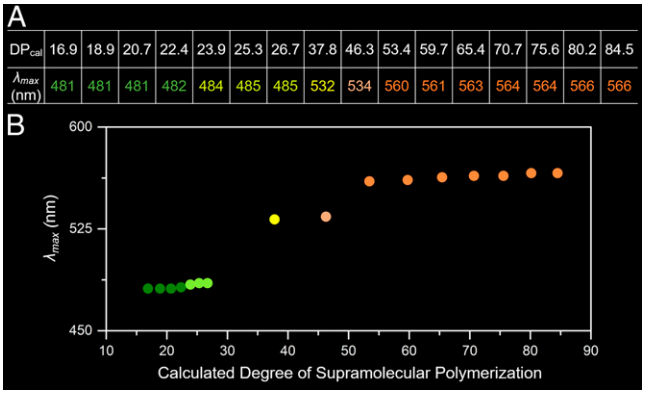

DP$_{cal}$	16.9	18.9	20.7	22.4	23.9	25.3	26.7	37.8	46.3	53.4	59.7	65.4	70.7	75.6	80.2	84.5
λ_{max} (nm)	481	481	481	482	484	485	485	532	534	560	561	563	564	564	566	566

Fig. 5. Relationship between λ_{max} and DP$_{cal}$. (*A*) Table and (*B*) plot of the corresponding dependent correlation between λ_{max} and DP$_{cal}$.

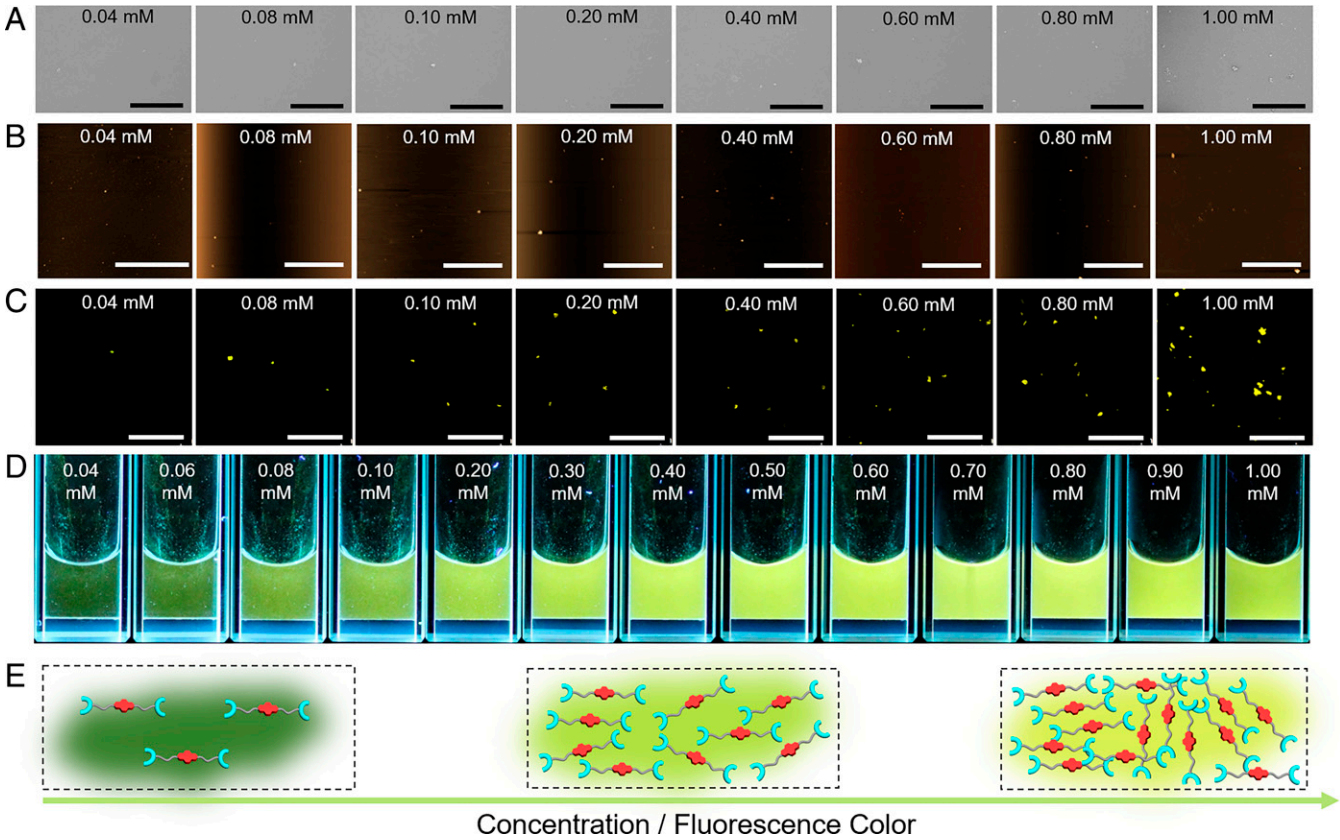

Fig. 6. Morphology, fluorescence behavior, and origin of the **M1**-derived fluorescence. (*A*) SEM images, (*B*) AFM images, and (*C*) LSCM images of **M1** solutions at different concentrations (0.04, 0.08, 0.10, 0.20, 0.40, 0.60, 0.80, and 1.00 mM in DMF/H_2O [1/4, vol/vol]). λ_{ex} = 405 nm. (*D*) Photographs of **M1** solutions (0.04 to 1.00 mM) recorded using a hand-held UV lamp. (*E*) Cartoon representations showing the various limiting self-assembled form of **M1** and the fluorescence color changes expected as the concentration of the monomers is increased. (Scale bars: *A*, 100 μm; *B*, 20.0 μm; *C*, 100 μm.)

colored images (Fig. 6*D*). These analyses revealed (Fig. 6*C*) that the number and size of the particles increased gradually with increasing **M1** concentration; however, no evidence of supramolecular polymer formation was seen. At low concentrations these particles were green in color and became yellow-green color at higher concentrations as seen in the LSCM images. Specifically, no further obvious color transitions were seen in contrast to what was observed for the **M1** + $Zn(OTf)_2$ solutions.

Fluorescence Properties of Monomer M1. The fluorescent colors of **M1** solutions at various concentrations were also recorded under UV light. As shown in Fig. 6*D* and Movie S2, as the **M1** concentration was increased from 0.04 mM to 0.10 mM and then to 0.20 mM, the fluorescent color evolved from dark green to green to yellow-green. We thus conclude that at higher concentrations the monomeric form of **M1** exists in equilibrium with stacked dimeric structures as illustrated in Fig. 6*E*. As the relative concentration of dimers increases, the fluorescence color becomes increasing yellow-green. No evidence of the highly aggregated orange emissive form is seen.

The normalized fluorescence spectra of the **M1** solutions were also recorded at various concentrations. As shown in Fig. 7, an increase in the **M1** concentration from 0.04 mM to 1.00 mM leads to a shift in the **M1** emission maximum from 481 nm to 525 nm. This net 44 nm shift in the λ_{max} is significantly lower than the difference in λ_{max} (85 nm) seen for equimolar solutions of **M1** + $Zn(OTf)_2$ as the concentration is similarly increased. Additionally, a yellow-green fluorescence is seen for 0.50 mM to 1.00 mM solutions of **M1**; in contrast, corresponding solutions of **M1** + $Zn(OTf)_2$ are characterized by an orange fluorescence emission. Taken in concert, these results provide support for the suggestion that supramolecular polymerization occurs in the case of **M1** + $Zn(OTf)_2$ in DMF/H_2O (1/4, vol/vol), but not for solutions of **M1** alone.

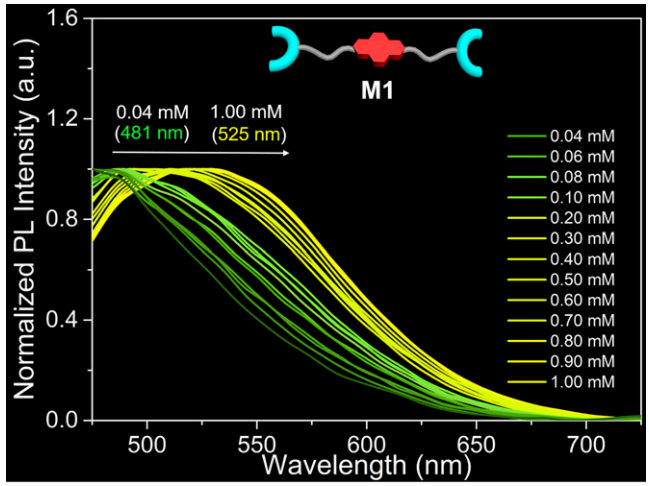

Fig. 7. Fluorescence characterization of **M1**. Normalized fluorescent spectra of solutions of **M1** recorded from 0.04 to 1.00 mM in DMF/H_2O (1/4, vol/vol) at 298 K. λ_{ex} = 410 nm. Slit: 10/15.

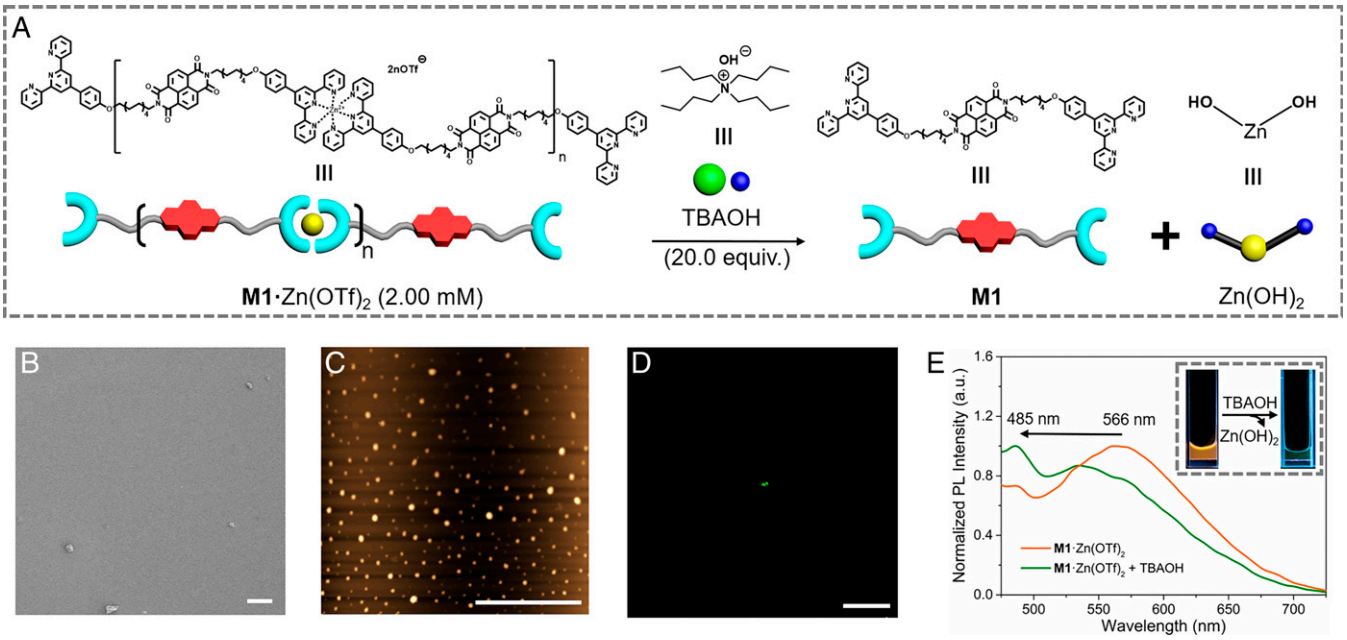

Fig. 8. Reaction mechanism, morphology, and fluorescence behavior of **M1** + $Zn(OTf)_2$ and TBAOH. (*A*) Cartoon representations of the reaction mechanism between $[\mathbf{M1}{\cdot}Zn(OTf)_2]_n$ (2.00 mM) and 20.0 equiv. of TBAOH (5.00 mM), both in DMF/H_2O (1/4, vol/vol). (*B*) SEM image, (*C*) AFM image, and (*D*) LSCM image of **M1** + $Zn(OTf)_2$ in DMF/H_2O (1/4, vol/vol) before and after the addition of TBAOH. (*E*) Normalized fluorescent spectra of **M1** + $Zn(OTf)_2$ (2.00 mM) and a mixture **M1** + $Zn(OTf)_2$ (2.00 mM) and TBAOH (5.00 mM) at 298 K. λ_{ex} = 410 nm. (*Inset*) Photographs of **M1** + $Zn(OTf)_2$ in DMF/H_2O (1/4, vol/vol) before and after the addition of TBAOH recorded under a hand-held UV lamp. Slit: 10/15. (Scale bars: *B*, 20.0 μm; *C*, 20.0 μm; *D*, 100 μm.)

Anion Responsiveness of $[\mathbf{M1}{\cdot}Zn(OTf)_2]_n$. We next sought to test whether the supramolecular polymer $[\mathbf{M1}{\cdot}Zn(OTf)_2]_n$ would display anion-responsive disaggregation behavior. Since the distinctive fluorescent properties of $[\mathbf{M1}{\cdot}Zn(OTf)_2]_n$ were attributed to stacked structures involving the NDI groups, it was expected that anion-induced depolymerization, to the extent it occurred, would be reflected in a readily discernible change in the fluorescent properties of the system. To test this proposition, TBAOH was added to preformed solutions $[\mathbf{M1}{\cdot}Zn(OTf)_2]_n$. According to previous reports (81), the OH^- anion was expected to interact strongly with the Zn^{2+} cation to form $Zn(OH)_2$ (Fig. 8*A*), thus breaking up the chelate complexes that provides the stabilization for the supramolecular polymer $[\mathbf{M1}{\cdot}Zn(OTf)_2]_n$. Upon addition of 20.0 equiv. of OH^- to a 2.00 mM solution of **M1** + $Zn(OTf)_2$, only granular species were seen by SEM (Fig. 8*B*) and AFM (Fig. 8*C*). Additionally, only green particles were observed in the corresponding LSCM images (Fig. 8*D*), rather than the orange fibrous species seen for $[\mathbf{M1}{\cdot}Zn(OTf)_2]_n$ in the absence of TBAOH. Moreover, after adding OH^- (20.0 equiv.) to a 2.00 mM solution of **M1** + $Zn(OTf)_2$ and removing the precipitate that formed (presumed to be zinc hydroxide), the color of the fluorescent solution changed from orange to green when irradiated with a hand-held UV lamp. Finally, as shown in Fig. 8*E*, incorporation of TBAOH also provoked a blue shift in the λ_{max} from 566 nm to 485 nm. On the basis of these combined results we conclude that the OH^- anion acts as a stimulus that depolymerizes $[\mathbf{M1}{\cdot}Zn(OTf)_2]_n$, thereby inducing a readily discernible change in the fluorescent color. This change in color can, in turn, be used to monitor the breakup of the *J*-aggregates present in the initial supramolecular polymer.

Conclusion

In conclusion, we present here two supramolecular monomers, a terpyridine modified NDI (**M1**) and $Zn(OTf)_2$, which can self-assemble into aggregated species driven by the coordination between terpyridine and $Zn(OTf)_2$. The formation of an anion-responsive supramolecular polymer. $[\mathbf{M1}{\cdot}Zn(OTf)_2]_n$, at higher concentrations was inferred on the basis of UV-vis spectroscopic titrations, as well as viscosity, SEM, AFM, and LSCM studies. Based on theoretical estimates, an increase in monomer concentration from 0.08 mM to 2.00 mM was expected to lead to an increase in the DP_{cal} from 16.9 to 84.5. Over this concentration range, a change in the fluorescent colors from green to yellow to orange, corresponding to a shift in λ_{max} from 481 nm to 566 nm, was observed by experiment. A dependent relationship between DP_{cal} and λ_{max} was established by combining the data for monomer concentration, DP_{cal}, and λ_{max}. As the DP_{cal} increased from 16.9 to 37.8 and then to 84.5, the λ_{max} of **M1** + $Zn(OTf)_2$ (as a DMF/H_2O (1/4, vol/vol) solution) shifted from 481 (green) to 532 (yellow) and then to 566 nm (orange). These spectral shifts were rationalized in terms of the supramolecular assembly-induced aggregation of NDI groups. With increasing monomer concentration, cyclic species/oligomers were firstly transformed to supramolecular polymers, and then to more fully entangled polymer-containing ensembles. These self-assembly processes, in turn, lead to a reduction in the distance between individual NDI groups, as **M1**-containing monomers are converted to dimeric forms and then to *J*-aggregated forms. Conversely, the specific addition of a hydroxide anion source to preformed $[\mathbf{M1}{\cdot}Zn(OTf)_2]_n$ was found to induce depolymerization and to restore the original fluorescence signature. Finally, the combination of different colors and fluorescence spectral features allowed changes in the DP_{cal} and corresponding differences in the supramolecular polymer molecular weights to be distinguished visually. The present optical-based differentiation strategy is expected to be generalizable and may prove useful in the characterization of supramolecular polymers containing appropriately chosen fluorophores.

Materials and Methods

Full experimental details and procedures for the synthesis of the compounds used in the present study, molecular structures, viscosity studies of **M1** + $Zn(OTf)_2$ solutions and **M1** solutions, preparation of **M1** + $Zn(OTf)_2$ solutions

and **M1** solutions, and details of the complexation study between **1a** and $Zn(OTf)_2$ are described in the *SI Appendix*.

Data Availability. All study data are included in the article and/or supporting information.

ACKNOWLEDGMENTS. X.J. acknowledges funding from the National Natural Science Foundation of China (No. 22001087). X.J. is grateful for support from the Huazhong University of Science and Technology, where he is being supported by Fundamental Research Funds for the Central Universities (grant 2020kfyXJJS013). X.J. also appreciates support from the Open Fund of Hubei Key Laboratory of Material Chemistry and Service Failure, Huazhong University of Science and Technology (2020MCF08). X.J. thanks the Chinese Ministry of Education for an Open Research Fund grant (No. 2021JYBKF01) to the Key Laboratory of Materials Chemistry for Energy Conversion and Storage (HUST). J.L.S. thanks the Robert A. Welch Foundation for Chair support (F-0018).

1. H. J. M. A. Mieras, C. F. H. V. Rijn, Elastic behaviour of low molecular weight polystyrenes. *Nature* **224**, 165–166 (1969).
2. A. Charlesby, Effect of molecular weight on the cross-linking of siloxanes by high-energy radiation. *Nature* **173**, 679–680 (1954).
3. K. Patel, S. H. Chikkali, S. Sivaram, Ultrahigh molecular weight polyethylene: Catalysis, structure, properties, processing and applications. *Prog. Polym. Sci.* **109**, 101290 (2020).
4. T. Deplancke, O. Lame, F. Rousset, R. Seguela, G. Vigier, Mechanisms of chain reentanglement during the sintering of UHMWPE nascent powder: Effect of molecular weight. *Macromolecules* **48**, 5328–5338 (2015).
5. T. Kida, Y. Hiejima, K.-h. Nitta, Microstructural interpretation of influences of molecular weight on the tensile properties of high-density polyethylene solids using Rheo-Raman spectroscopy. *Macromolecules* **54**, 225–234 (2021).
6. L. Brunsveld, B. J. B. Folmer, E. W. Meijer, R. P. Sijbesma, Supramolecular polymers. *Chem. Rev.* **101**, 4071–4098 (2001).
7. T. F. A. de Greef, E. W. Meijer, Materials science: Supramolecular polymers. *Nature* **453**, 171–173 (2008).
8. C. Fouquey, J.-M. Lehn, A.-M. Levelut, Molecular recognition directed self-assembly of supramolecular liquid crystalline polymers from complementary chiral components. *Adv. Mater.* **2**, 254–257 (1990).
9. K. V. Rao *et al.*, Distinct pathways in "thermally bisignate supramolecular polymerization": Spectroscopic and computational studies. *J. Am. Chem. Soc.* **142**, 598–605 (2020).
10. L. Xu *et al.*, Metallacycle-cored supramolecular polymers: Fluorescence tuning by variation of substituents. *J. Am. Chem. Soc.* **140**, 16920–16924 (2018).
11. A. Lavrenova *et al.*, Mechano- and thermoresponsive photoluminescent supramolecular polymer. *J. Am. Chem. Soc.* **139**, 4302–4305 (2017).
12. P. Kuad, A. Miyawaki, Y. Takashima, H. Yamaguchi, A. Harada, External stimulus-responsive supramolecular structures formed by a stilbene cyclodextrin dimer. *J. Am. Chem. Soc.* **129**, 12630–12631 (2007).
13. P. Wei, X. Yan, F. Huang, Supramolecular polymers constructed by orthogonal self-assembly based on host-guest and metal-ligand interactions. *Chem. Soc. Rev.* **44**, 815–832 (2015).
14. S. Dong, B. Zheng, F. Wang, F. Huang, Supramolecular polymers constructed from macrocycle-based host-guest molecular recognition motifs. *Acc. Chem. Res.* **47**, 1982–1994 (2014).
15. Y. Han, Y. Tian, Z. Li, F. Wang, Donor-acceptor-type supramolecular polymers on the basis of preorganized molecular tweezers/guest complexation. *Chem. Soc. Rev.* **47**, 5165–5176 (2018).
16. L. Wang *et al.*, A self-cross-linking supramolecular polymer network enabled by crown-ether-based molecular recognition. *J. Am. Chem. Soc.* **142**, 2051–2058 (2020).
17. S.-L. Li, T. Xiao, C. Lin, L. Wang, Advanced supramolecular polymers constructed by orthogonal self-assembly. *Chem. Soc. Rev.* **41**, 5950–5968 (2012).
18. B. Li, T. He, X. Shen, D. Tang, S. Yin, Fluorescent supramolecular polymers with aggregation induced emission properties. *Polym. Chem.* **10**, 796–818 (2019).
19. Z.-Y. Li *et al.*, Cross-linked supramolecular polymer gels constructed from discrete multi-pillar[5]arene metallacycles and their multiple stimuli-responsive behavior. *J. Am. Chem. Soc.* **136**, 8577–8589 (2014).
20. H.-Y. Gong *et al.*, Environmentally responsive threading, dethreading, and fixation of anion-induced pseudorotaxanes. *J. Am. Chem. Soc.* **133**, 1526–1533 (2011).
21. B. Qin *et al.*, Supramolecular interfacial polymerization: A controllable method of fabricating supramolecular polymeric materials. *Angew. Chem. Int. Ed. Engl.* **56**, 7639–7643 (2017).
22. Y. Zhu, W. Zheng, W. Wang, H.-B. Yang, When polymerization meets coordination-driven self-assembly: Metallo-supramolecular polymers based on supramolecular coordination complexes. *Chem. Soc. Rev.* **50**, 7395–7417 (2021).
23. P. Xing *et al.*, Occurrence of chiral nanostructures induced by multiple hydrogen bonds. *J. Am. Chem. Soc.* **141**, 9946–9954 (2019).
24. E. M. Todd, S. C. Zimmerman, Supramolecular star polymers. Increased molecular weight with decreased polydispersity through self-assembly. *J. Am. Chem. Soc.* **129**, 14534–14535 (2007).
25. X. Wang *et al.*, Cooperative supramolecular polymerization of fluorescent platinum acetylides for optical waveguide applications. *Angew. Chem. Int. Ed. Engl.* **56**, 12466–12470 (2017).
26. X. Yan *et al.*, Responsive supramolecular polymer metallogel constructed by orthogonal coordination-driven self-assembly and host/guest interactions. *J. Am. Chem. Soc.* **136**, 4460–4463 (2014).
27. Q. He, P. Tu, J. L. Sessler, Supramolecular chemistry of anionic dimers, trimers, tetramers, and clusters. *Chem* **4**, 46–93 (2018).
28. X. Ji, X. Chi, M. Ahmed, L. Long, J. L. Sessler, Soft materials constructed using calix[4]pyrrole- and "texas-sized" box-based anion receptors. *Acc. Chem. Res.* **52**, 1915–1927 (2019).
29. E. S. Silver, B. M. Rambo, C. W. Bielawski, J. L. Sessler, Reversible anion-induced cross-linking of well-defined calix[4]pyrrole-containing copolymers. *J. Am. Chem. Soc.* **136**, 2252–2255 (2014).
30. H. Wang *et al.*, Constraining homo- and heteroanion dimers in ultraclose proximity within a self-assembled hexacationic cage. *J. Am. Chem. Soc.* **142**, 20182–20190 (2020).
31. Z. Zhang *et al.*, Expanded porphyrin-anion supramolecular assemblies: Environmentally responsive sensors for organic solvents and anions. *J. Am. Chem. Soc.* **137**, 7769–7774 (2015).
32. W. Chen *et al.*, Molecular cursor caliper: A fluorescent sensor for dicarboxylate dianions. *J. Am. Chem. Soc.* **141**, 14798–14806 (2019).
33. F. Wang *et al.*, Self-assembled cagelike receptor that binds biologically relevant dicarboxylic acids via proton-coupled anion recognition. *J. Am. Chem. Soc.* **142**, 1987–1994 (2020).
34. J. Yang *et al.*, Excimer disaggregation enhanced emission: A fluorescence "turn-on" approach to oxoanion recognition. *J. Am. Chem. Soc.* **141**, 4597–4612 (2019).
35. X. Ji *et al.*, Physical removal of anions from aqueous media by means of a macrocycle-containing polymeric network. *J. Am. Chem. Soc.* **140**, 2777–2780 (2018).
36. S. Peng *et al.*, Strapped calix[4]pyrroles: From syntheses to applications. *Chem. Soc. Rev.* **49**, 865–907 (2020).
37. N. Busschaert, C. Caltagirone, W. Van Rossom, P. A. Gale, Applications of supramolecular anion recognition. *Chem. Rev.* **115**, 8038–8155 (2015).
38. P. Molina, F. Zapata, A. Caballero, Anion recognition strategies based on combined noncovalent interactions. *Chem. Rev.* **117**, 9907–9972 (2017).
39. W. Chen *et al.*, β-Cyclodextrin modified Pt(II) metallacycle-based supramolecular hyperbranched polymer assemblies for DOX delivery to liver cancer cells. *Proc. Natl. Acad. Sci. U.S.A.* **117**, 30942–30948 (2020).
40. G. Liu *et al.*, Controlling supramolecular chirality of two-component hydrogels by *J*- and *H*-aggregation of building blocks. *J. Am. Chem. Soc.* **140**, 6467–6473 (2018).
41. G. Liu *et al.*, Control on dimensions and supramolecular chirality of self-assemblies through light and metal ions. *J. Am. Chem. Soc.* **140**, 16275–16283 (2018).
42. J. Cai, J. L. Sessler, Neutral CH and cationic CH donor groups as anion receptors. *Chem. Soc. Rev.* **43**, 6198–6213 (2014).
43. A. Winter, U. S. Schubert, Synthesis and characterization of metallo-supramolecular polymers. *Chem. Soc. Rev.* **45**, 5311–5357 (2016).
44. L. Yang, X. Tan, Z. Wang, X. Zhang, Supramolecular polymers: Historical development, preparation, characterization, and functions. *Chem. Rev.* **115**, 7196–7239 (2015).
45. Y. Liu, Z. Wang, X. Zhang, Characterization of supramolecular polymers. *Chem. Soc. Rev.* **41**, 5922–5932 (2012).
46. R. B. Martin, Comparisons of indefinite self-association models. *Chem. Rev.* **96**, 3043–3064 (1996).
47. M. E. Cates, Reptation of living polymers: Dynamics of entangled polymers in the presence of reversible chain-scission reactions. *Macromolecules* **20**, 2289–2296 (1987).
48. S. Abed, S. Boileau, L. Bouteiller, Supramolecular association of acid terminated polydimethylsiloxanes. 3. Viscosimetric study. *Polymer (Guildf.)* **42**, 8613–8619 (2001).
49. R. P. Sijbesma *et al.*, Reversible polymers formed from self-complementary monomers using quadruple hydrogen bonding. *Science* **278**, 1601–1604 (1997).
50. M. Miyauchi, Y. Takashima, H. Yamaguchi, A. Harada, Chiral supramolecular polymers formed by host-guest interactions. *J. Am. Chem. Soc.* **127**, 2984–2989 (2005).
51. Y. Hasegawa, M. Miyauchi, Y. Takashima, H. Yamaguchi, A. Harada, Supramolecular polymers formed from β-cyclodextrins dimer linked by poly(ethylene glycol) and guest dimers. *Macromolecules* **38**, 3724–3730 (2005).
52. F. Huang, H. W. Gibson, A supramolecular poly[3]pseudorotaxane by self-assembly of a homoditopic cylindrical bis(crown ether) host and a bisparaquat derivative. *Chem. Commun. (Camb.)* **2005**, 1696–1698 (2005).
53. F. Huang, H. W. Gibson, Formation of a supramolecular hyperbranched polymer from self-organization of an AB2 monomer containing a crown ether and two paraquat moieties. *J. Am. Chem. Soc.* **126**, 14738–14739 (2004).
54. H. W. Gibson, N. Yamaguchi, J. W. Jones, Supramolecular pseudorotaxane polymers from complementary pairs of homoditopic molecules. *J. Am. Chem. Soc.* **125**, 3522–3533 (2003).
55. X. Zhang, C. Liu, Z. Wang, Force spectroscopy of polymers: Studying on intramolecular and intermolecular interactions in single molecular level. *Polymer (Guildf.)* **49**, 3353–3361 (2008).
56. D. Bialas, E. Kirchner, M. I. S. Röhr, F. Würthner, Perspectives in dye chemistry: A rational approach toward functional materials by understanding the aggregate state. *J. Am. Chem. Soc.* **143**, 4500–4518 (2021).
57. M. Hecht, F. Würthner, Supramolecularly engineered *J*-aggregates based on perylene bisimide dyes. *Acc. Chem. Res.* **54**, 642–653 (2021).

58. Z. Chen, A. Lohr, C. R. Saha-Möller, F. Würthner, Self-assembled π-stacks of functional dyes in solution: Structural and thermodynamic features. *Chem. Soc. Rev.* **38**, 564–584 (2009).
59. N. J. Hestand, F. C. Spano, Expanded theory of H- and J-molecular aggregates: The effects of vibronic coupling and intermolecular charge transfer. *Chem. Rev.* **118**, 7069–7163 (2018).
60. M. A. Kobaisi, S. V. Bhosale, K. Latham, A. M. Raynor, S. V. Bhosale, Functional naphthalene diimides: Synthesis, properties, and applications. *Chem. Rev.* **116**, 11685–11796 (2016).
61. A. Takai *et al.*, Supramolecular assemblies of ferrocene-hinged naphthalenediimides: Multiple conformational changes in film states. *J. Am. Chem. Soc.* **138**, 11245–11253 (2016).
62. Y. Hong *et al.*, Fluorogenic Zn(II) and chromogenic Fe(II) sensors based on terpyridine-substituted tetraphenylethenes with aggregation-induced emission characteristics. *ACS Appl. Mater. Interfaces* **3**, 3411–3418 (2011).
63. Y.-Y. Zhang *et al.*, A highly sensitive multifunctional sensor based on phenylene-acetylene for colorimetric detection of Fe^{2+} and ratiometric fluorescent detection of Cd^{2+} and Zn^{2+}. *Sens. Actuators B Chem.* **273**, 1077–1084 (2018).
64. R. Singh *et al.*, Optical-switchable energy transfer controlled by multiple-responsive turn-on fluorescence via metal–ligand and host–guest interactions in diarylethene-based [2]pseudo-rotaxane polymers. *Mater. Chem. Front.* **5**, 438–449 (2021).
65. P. Thordarson, Determining association constants from titration experiments in supramolecular chemistry. *Chem. Soc. Rev.* **40**, 1305–1323 (2011).
66. R. Dobrawa, M. Lysetska, P. Ballester, M. Grüne, F. Würthner, Fluorescent supramolecular polymers: Metal directed self-assembly of perylene bisimide building blocks. *Macromolecules* **38**, 1315–1325 (2005).
67. H. A. Benesi, J. H. Hildebrand, A spectrophotometric investigation of the interaction of iodine with aromatic hydrocarbons. *J. Am. Chem. Soc.* **71**, 2703–2707 (1949).
68. Q. Zhang *et al.*, Self-healing heterometallic supramolecular polymers constructed by hierarchical assembly of triply orthogonal interactions with tunable photophysical properties. *J. Am. Chem. Soc.* **141**, 17909–17917 (2019).
69. X. Ji *et al.*, pH-responsive supramolecular polymerization in aqueous media driven by electrostatic attraction-enhanced crown ether-based molecular recognition. *Macromol. Rapid Commun.* **33**, 1197–1202 (2012).
70. Y. Ding, P. Wang, Y.-K. Tian, Y.-J. Tian, F. Wang, Formation of stimuli-responsive supramolecular polymeric assemblies via orthogonal metal-ligand and host-guest interactions. *Chem. Commun. (Camb.)* **49**, 5951–5953 (2013).
71. Y.-K. Tian, L. Chen, Y.-J. Tian, X.-Y. Wang, F. Wang, Controlled formation of a supramolecular polymer network driven by heterometallic coordination interactions. *Polym. Chem.* **4**, 453–457 (2013).
72. A. Kumar, S. Bawa, K. Ganorkar, S. K. Ghosh, A. Bandyopadhyay, Syntheses, characterization, multi-acid fluorescence sensing and electroluminescence properties of Cr(II)-based metallopolymers. *Polym. Chem.* **11**, 6579–6590 (2020).
73. A. Frank *et al.*, Hierarchical superstructures by combining crystallization-driven and molecular self-assembly. *Angew. Chem. Int. Ed. Engl.* **60**, 21767–21771 (2021).
74. K. Venkata Rao, D. Miyajima, A. Nihonyanagi, T. Aida, Thermally bisignate supramolecular polymerization. *Nat. Chem.* **9**, 1133–1139 (2017).
75. T. Fukushima *et al.*, Diarylethene-powered light-induced folding of supramolecular polymers. *J. Am. Chem. Soc.* **143**, 5845–5854 (2021).
76. N. Bäumer *et al.*, Tuning energy landscapes and metal-metal interactions in supramolecular polymers regulated by coordination geometry. *Chem. Sci. (Camb.)* **12**, 5236–5245 (2021).
77. Z. M. Hudson, D. J. Lunn, M. A. Winnik, I. Manners, Colour-tunable fluorescent multiblock micelles. *Nat. Commun.* **5**, 3372 (2014).
78. A. Aliprandi, M. Mauro, L. De Cola, Controlling and imaging biomimetic self-assembly. *Nat. Chem.* **8**, 10–15 (2016).
79. V. Dehm *et al.*, Helical growth of semiconducting columnar dye assemblies based on chiral perylene bisimides. *Org. Lett.* **9**, 1085–1088 (2007).
80. J. Price, B. Balónová, B. A. Blight, S. Eisler, Shedding light on predicting and controlling emission chromaticity in multicomponent photoluminescent systems. *Chem. Sci. (Camb.)* **12**, 12092–12097 (2021).
81. B. Gruber, E. Kataev, J. Aschenbrenner, S. Stadlbauer, B. König, Vesicles and micelles from amphiphilic zinc(II)-cyclen complexes as highly potent promoters of hydrolytic DNA cleavage. *J. Am. Chem. Soc.* **133**, 20704–20707 (2011).